JOURNAL OF AIRCRAFT
Vol. 30, No. 5, Sept.–Oct. 1993

# Vector Unsymmetric Eigenequation Solver for Nonlinear Flutter Analysis on High-Performance Computers

Jiangning Qin*
*Old Dominion University, Norfolk, Virginia 23529*
Carl E. Gray Jr.†
*NASA Langley Research Center, Hampton, Virginia 23665*
and
Chuh Mei‡
*Old Dominion University, Norfolk, Virginia 23529*

**An efficient, vector-version generalized unsymmetric eigenequation solver is developed for large-amplitude vibration and nonlinear panel flutter analyses by finite-element methods on high-performance computers. The proposed eigensolver is designed to extract extreme eigenpairs which are all that are required in solving panel flutter problems. A loop-unrolling technique is employed to enhance the vector speed of the eigensolver. A finite-element approach is presented for determining the nonlinear flutter characteristics of isotropic and composite panels using unsteady, third-order piston theory aerodynamics. Both nonlinear structural (large-amplitude, and nonlinear aerodynamics terms are considered in the finite-element formulation. Solution procedures are presented to solve the nonlinear panel flutter and large amplitude-free vibration finite-element equations. Nonlinear flutter analyses are performed for different dynamic pressures $\lambda$; and maximum deflection-to-thickness ratios $c/h$. Large-amplitude vibration finite-element results are compared with classical analytical solutions. Nonlinear aerodynamic and linear structural finite-element flutter results for composite panels are also presented.**

## I. Introduction

PANEL flutter is the self-excited or self-sustained oscillation of an external panel of a flight vehicle when exposed to supersonic or hypersonic airflow. This type of flutter differs from wing flutter in that the aerodynamic forces resulting from the airflow act only on one side of the panel. In the context of small deflection (linear) structural theory, there is a critical value of the nondimensional dynamic pressure parameter $\lambda_{cr}$ (or flow velocity) above which the panel motion becomes unstable and grows exponentially with time. Below this critical dynamic pressure, any disturbance to the panel results in motion that decays exponentially with time. A vast quantity of literature exists on linear panel flutter using different aerodynamic theories (e.g., Refs. 1–3 and many others). For panel flutter at high supersonic Mach numbers ($M_\infty > 1.7$), the aerodynamic theory applied for the most part is a quasisteady first-order piston theory aerodynamics.[4] Because of the resurgent interest in flight vehicles such as the high-speed civil transport (HSCT), the national aero-space plane (NASP), and the advanced tactical fighter (ATF) that will operate not only at high-supersonic Mach numbers but well into the hypersonic regime, the proposed finite-element approach employs unsteady nonlinear third-order piston theory aerodynamics. This aerodynamic theory has been employed to approximate the aerodynamic loads on the panel from local pressures generated by the body's motion as related to the local normal component of the fluid velocity; thus, a point-function relationship between the normal component of the fluid velocity and the local panel pressure is obtained. For high supersonic Mach numbers, this theory has been shown to reasonably estimate the aerodynamic pressures.[2]

In actuality, the panel not only bends, but also stretches due to large-amplitude vibrations. Membrane tensile forces in the panel, due to the induced stretching, provide a limited stabilizing effect of the "hard spring" type that restrains the panel motion to a bounded amplitude for limit-cycle oscillations with increasing amplitude as the dynamic pressure increases. Therefore, the external skin of a flight vehicle can withstand flow velocities beyond the linear critical value $\lambda_{cr}$. McIntosh[5] investigated the effects of hypersonic nonlinear aerodynamic loadings on two-dimensional isotropic panel flutter. His findings show that the higher-order piston theory aerodynamics may, for some system parameters, produce a "soft spring" effect that will predict lower flutter velocities. Two notable surveys on the subject of linear and nonlinear panel flutter are given by Dowell[6] and, most recently by Reed et al.[7]

Because of the resurgent interest in panel flutter at the high-supersonic/hypersonic speeds,[7] this article extends the finite-element method to investigate the limit-cycle oscillations of composite panels subject to hypersonic flow as described by the third-order piston theory aerodynamics. In doing so, an efficient unsymmetric eigensolver is required, because only the first few eigenpairs are needed. The two most powerful methods for the partial solution of symmetric eigenproblems are the subspace iteration method[8] and the Lanczos method.[9,10] These methods have been extended for unsymmetric eigenproblems, such as the unsymmetric subspace iteration method[11] and the unsymmetric Lanczos method.[12,13] Unfortunately, if there are complex eigenpairs, such as in the nonlinear panel flutter analysis, these methods require computations in the complex domain, and therefore, increase the computational cost and complexity. Moreover, the unsymmetric Lanczos method requires two starting vectors and has the so-called "breakdown" problem.[14]

In this article an eigensolver for the reduced solution-space of an unsymmetric eigenproblems is proposed which trans-

Presented as Paper 91-1169 at the AIAA/ASME/ASCE/AHS/ASC 32nd Structures, Structural Dynamics, and Materials Conference, Baltimore, MD, April 8–10, 1991; received Oct. 21, 1991; revision received April 13, 1992; accepted for publication May 21, 1992. 

*Research Associate, Department of Mechanical Engineering and Mechanics. Member AIAA.
†Aerospace Engineer, Facilities Engineering Division. Senior Member AIAA.
‡Professor, Department of Mechanical Engineering and Mechanics. Associate Fellow AIAA.

forms the original matrix of order $n \times n$ to an upper Hessenburg matrix of reduced order $m \times m$ ($m << n$) by means of orthogonal reduction. The eigenpairs of the reduced system are obtained very efficiently, and then they are transformed back to obtain the approximate eigenpairs of the original system. All the computations involved are in the real domain, and only one started vector is required. Numerical techniques including refining the starting vector and reorthogonalization of the base vectors are introduced in this method to improve both accuracy and convergency. The proposed eigensolver is also vectorized for the applications on high-performance computers. Special data storage scheme and loop-unrolling technique are developed to fully exploit the vector capability provided by modern supercomputers. Numerical results obtained for the nonlinear composite panel flutter analysis are presented to demonstrate the efficiency and accuracy of this unsymmetric eigensolver method.

## II. Finite-Element Formulation

Consider a flat panel of length $a$, width $b$, thickness $h$, and mass density $\rho$, with air flowing above the panel at Mach number $M_\infty$, shown in Fig. 1. It is assumed that the air flowing above the panel is in the positive $x$ direction and that the cavity effects on the back side of the panel can be neglected. The sign convention to be followed is that a positive flow direction is in the increasing $x$ direction and that a positive deflection is into the cavity.

### A. Hamilton's Principle for a Continuum

The general form of Hamilton's principle for a nonconservative, elastic, continuous medium is

$$\int_{t_1}^{t_2} \left\{ \int_V (\rho \boldsymbol{u}_{,tt} \cdot \delta \boldsymbol{u}\, dV) - \left[ \int_V (\boldsymbol{f} \cdot \delta \boldsymbol{u}\, dV) + \int_S (\boldsymbol{p} \cdot \delta \boldsymbol{u}\, dS) - \int_V \sigma : \delta\varepsilon\, dV \right] \right\} dt = 0 \tag{1}$$

The terms under the time integral represent the work done on the body at any time $t$ by the resultant force in moving through the virtual displacement $\delta \boldsymbol{u}$; $\boldsymbol{f}$ is the body force, and is neglected in this formulation; $\boldsymbol{p}$ is the specified surface stress vector, and $\sigma : \delta\varepsilon$ is a stress-virtual strain-tensor product.

### B. Constitutive and Strain-Displacement Relationships

For an orthotropic lamina,[15] the stress-strain relationship in the material coordinate system becomes

$$\{\sigma\} = [Q]\{\varepsilon\} \tag{2}$$

where $[Q]$ is the reduced stiffness. Similarly the form of the strain-displacement relationships for an arbitrary point of coordinate $z$ through the panel thickness $h$ is

$$\begin{aligned} \varepsilon_x &= u_{,x} + \tfrac{1}{2} w_{,x}^2 - z w_{,xx} \\ \varepsilon_y &= v_{,y} + \tfrac{1}{2} w_{,y}^2 - z w_{,yy} \\ \varepsilon_{xy} &= u_{,y} + v_{,x} + w_{,x} w_{,y} - 2z w_{,xy} \end{aligned} \tag{3}$$

### C. Aerodynamic Pressure Function

The virtual work integral involving the surface stress vector is evaluated using the unsteady full third-order piston theory aerodynamics[4,5] to develop the aerodynamic loads on the upper surface of the panel. Again, this relates the local point function pressure generated by the panel's motion to the local normal component of the flow velocity. Thus, the aerodynamic pressure loading as given by this theory is

$$\begin{aligned} p - p_\infty = (2q/M_\infty)\{&(1/V) w_{,t} + w_{,x} + [(1+\gamma)/4] M_\infty \\ &\cdot [(1/V) w_{,t} + w_{,x}]^2 + [(1+\gamma)/12] M_\infty^2 \\ &\cdot [(1/V) w_{,t} + w_{,x}]^3\} \end{aligned} \tag{4}$$

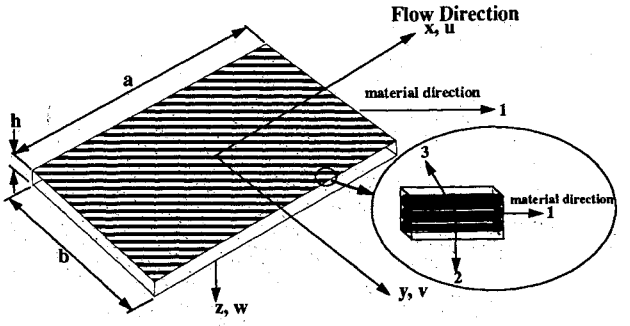


**Fig. 1 Panel geometry.**

where $q = \rho_a V^2/2$ is the dynamic pressure, $\rho_a$ is the air density, $V$ is the airflow speed, and $\gamma$ is the ratio of specific heat. The first two terms in Eq. (4) constitute what is commonly referred to as the first-order piston theory aerodynamics, whereas, Eq. (4) without the cubic term, represents the second-order piston theory aerodynamics.

### D. System Finite-Element Formulation and Solution Procedure

The variational principle in Eq. (1) represents a finite-element approach to study the limit-cycle oscillations of composite panels at hypersonic speeds. Unlike the first-order piston theory aerodynamics which will produce two linear aerodynamic influence matrices ($[G]$ and $[A]$), the third-order piston theory aerodynamics yields, in addition to the same two linear matrices, seven nonlinear aerodynamic damping and aerodynamic influence matrices ($[G1_t]$, $[G2_t]$, $[G2_{ft}]$, $[A1_t]$, $[A1_f]$, $[A2_f]$, and $[A2_{ft}]$). The subscripts $f$ and $t$ denote displacement and velocity (time derivative), respectively. These aerodynamic matrices are functions of the system aerodynamic parameters, in particular the nondimensional dynamic pressure, $\lambda (\lambda = 2qa^3/M_\infty D_c$, where $D_c = E_{11}h^3)$. The nonlinear aerodynamic matrices depend linearly ($[G1]$ and $[A1]$) and quadratically ($[G2]$ and $[A2]$) upon the panel's displacements and the time derivatives of the displacements (generalized velocities).

By assembling the individual finite elements for the entire system and applying the kinematic boundary conditions, the equations of motion for the coupled (bending/membrane) system are of the form, using the convention that upper case matrix notation pertains to the assembled structure

$$\begin{aligned} &\begin{bmatrix} [M_f] & [0] \\ [0] & [M_m] \end{bmatrix} \{\ddot{W}\} \\ &+ \begin{bmatrix} ([G] + [G1_t] + [G2_t] + [G2_{ft}]) & [0] \\ [0] & [0] \end{bmatrix} \{\dot{W}\} \\ &+ \begin{bmatrix} ([A] + [A1_t] + [A1_f] + [A2_f] + [A2_{ft}]) & [0] \\ [0] & [0] \end{bmatrix} \{W\} \\ &+ \begin{bmatrix} [K_{ff}] & [K_{Bfm}] \\ [K_{Bmf}] & [K_{mm}] \end{bmatrix} \{W\} + \begin{bmatrix} [K1_{ff}] & [K1_{fm}] \\ [K1_{mf}] & [0] \end{bmatrix} \{W\} \\ &+ \begin{bmatrix} [K1_{Bff}] & [0] \\ [0] & [0] \end{bmatrix} \{W\} \\ &+ \begin{bmatrix} [K2_f] & [0] \\ [0] & [0] \end{bmatrix} \{W\} = \{0\} \end{aligned} \tag{5}$$

where

$$\{W\} = \begin{Bmatrix} W_f \\ W_m \end{Bmatrix} \tag{6}$$

are the constrained nodal displacements of the assembled system, and the subscripts $f$ and $m$ denote flexural and membrane components, respectively. This matrix equation, as written, is a damped vibration problem in the configuration space, and as such, it does not lend itself to standard eigenvalue solution algorithms. Thus, the approach to be adopted transforms the system equations from the configuration solution space to the state space. This results in a more standard form of the eigenvalue problem. By making the transformation to the state space, the governing matrix equation [Eq. (5)] becomes

$$\begin{bmatrix} [M] & [0] \\ [0] & [I] \end{bmatrix} \begin{Bmatrix} \ddot{W} \\ \dot{W} \end{Bmatrix} + \begin{bmatrix} [G] & [K] \\ [-I] & [0] \end{bmatrix} \begin{Bmatrix} \dot{W} \\ W \end{Bmatrix} = \{0\} \tag{7}$$

where $[M]$ is the system mass matrix, $[G]$ is the system aerodynamic damping matrix, $[K]$ incudes both the system stiffness and aerodynamic influence matrices, and $[I]$ is an identity matrix. The solution to the homogeneous problem is sought in the form of

$$\begin{Bmatrix} \dot{W} \\ W \end{Bmatrix} = \bar{c} \begin{Bmatrix} \Phi_1 \\ \Phi_2 \end{Bmatrix} e^{\Omega t} \tag{8}$$

where $\{\Phi_1\}$ and $\{\Phi_2\}$ are complex eigenvectors that are arranged as a single column vector, $\Omega = (\alpha + i\omega)$ is the complex eigenvalue, $\alpha$ is the damping rate, $\omega$ is the circular frequency, and $\bar{c}$ is a nonzero (scalar) constant displacement amplitude. Substituting the assumed response into Eq. (7) results in the following eigenvalue problem:

$$\bar{c}\left(\Omega \begin{bmatrix} [M] & [0] \\ [0] & [I] \end{bmatrix} + \begin{bmatrix} [G] & [K] \\ [-I] & [0] \end{bmatrix}\right) \begin{Bmatrix} \Phi_1 \\ \Phi_2 \end{Bmatrix} e^{\Omega t} = \{0\} \tag{9}$$

By expressing $e^{\Omega t}$ as a complex quantity in Euler form, and requiring both coefficients of $\sin(\omega t)$ and $\cos(\omega t)$ to vanish, then Eq. (9) can be written as two separate equations

$$\bar{c}e^{\alpha t}\left(\Omega \begin{bmatrix} [M] & [0] \\ [0] & [I] \end{bmatrix} + \begin{bmatrix} [G] & [K] \\ [-I] & [0] \end{bmatrix}\right) \begin{Bmatrix} \Phi_1 \\ \Phi_2 \end{Bmatrix} \cos(\omega t) = \{0\} \tag{10}$$

$$i\bar{c}e^{\alpha t}\left(\Omega \begin{bmatrix} [M] & [0] \\ [0] & [I] \end{bmatrix} + \begin{bmatrix} [G] & [K] \\ [-I] & [0] \end{bmatrix}\right) \begin{Bmatrix} \Phi_1 \\ \Phi_2 \end{Bmatrix} \sin(\omega t) = \{0\} \tag{11}$$

Since $\bar{c}$ is nonzero, Eq. (5) is for the constrained system, and the solution sought is for all times greater than zero, then both Eqs. (10) and (11) represent the same eigenvalue problem. To solve Eq. (10), the nonlinear matrices in Eq. (5) need to be evaluated. Also, since all of the system quantities used in developing Eq. (5) are real, it must be concluded that the nodal response quantities must also be real.[3] As is generally the case with most nonlinear problems, numerous methodologies are available to obtain linearized solutions. Thus, a significant focus of this study has been centered around efficiently solving the resulting nonlinear eigenvalue problem of Eq. (10) for synchronous motions. This can be accomplished by linearizing Eq. (7) and employing an iterative solution procedure developed in Ref. 16. The field expressions for the transverse panel displacement, velocity, and slope are denoted by $w$ and can be approximated from the element nodal quantities $\{w\}$, and element shape function for the transverse displacement $[\phi]$, as

$$w = [\phi]\{w_f\} \tag{12}$$

$$w_{,t} = [\phi]\{\dot{w}_f\} \tag{13}$$

$$w_{,x} = [\phi_{,x}]\{w_f\} \tag{14}$$

$$w_{,y} = [\phi_{,y}]\{w_f\} \tag{15}$$

Similar expressions can be developed for the inplane displacements $u$ and $v$. All of these quantities can be approximated from Eq. (8) by normalizing the eigenvector as follows (see Ref. 16 for a more detailed discussion), and recognizing that $\{w\}$ is a real quantity, and as such take only the real part of the normalized Eq. (8)

$$\begin{Bmatrix} \dot{W} \\ W \end{Bmatrix} = \frac{\bar{c}e^{\alpha t}}{|(\Phi_2)_k|} \begin{Bmatrix} |\Phi_1|\cos(\beta - \beta_k) \\ |\Phi_2|\cos(\beta - \beta_k) \end{Bmatrix} \cos(\omega t) \tag{16}$$

The quantity $|(\Phi_2)_k|$ is the magnitude of the largest displacement component of the eigenvector that corresponds to $\{W_f\}$, and $\beta_k$ is the corresponding phase angle. Next, denote $c = \bar{c}e^{\alpha t}$ as the damped amplitude. Thus, it is clear from Eq. (16) that the sign of the real part of the eigenvalue controls the stability of the solution. The solution is stable for all damping rate $\alpha$ that are less than zero. For $\alpha$ equal to zero, then $c$ equals $\bar{c}$, and the resulting solution corresponds to that of a limit-cycle oscillation.

If Eq. (8) is normalized, then it can be scaled to a given limit-cycle amplitude, $c$. Having normalized and scaled Eq. (8), then Eq. (16) results, and $u$, $v$, $w$, and their derivatives for each element can be easily computed. Next, by dropping the nonlinear terms in Eq. (7) and solving the linear eigenvalue problem, the first estimate of the nodal quantities can be approximated. With the linear eigenvectors, the process just described[16] can be used to approximate the quantities necessary to assemble the nonlinear element matrices and the assembled constrained system matrices. The same process can be repeated until successive iterations yield the same eigenvalues, both real and imaginary, and the same eigenvectors within the limits of a convergence criteria. Therefore, for a given panel configuration and dynamic pressure, the nonlinear system eigenvalues and eigenvectors can be computed.

As the dynamic pressure is increased monotonically from zero ($\lambda = 0$ corresponds to in-vacuo large-amplitude vibration), the symmetric, real, and positive definite stiffness matrix is perturbed by the skewed aerodynamic influence matrix so that two of the eigenvalues approach each other until they coalesce. A critical dynamic pressure $\lambda_{cr}$ for the linear structure ($c/h = 0$), and a limit-cycle dynamic pressure $\lambda_l$ for the nonlinear structure, are determined when the real part of the eigenvalue approaches positive values for a fixed dynamic pressure. A typical response curve for a linear, three-dimensional square panel is shown in Fig. 2.

At each value of $\lambda$, an iterative solution of Eq. (7) must be performed. Each converged solution for a fixed $\lambda$ generally requires 3–10 iterations. Thus, to determine the critical or limit-cycle dynamic pressure may require as many as 100 iterations. Couple this with the large number of degrees of freedom (DOF) to accurately model a fluttering composite panel, the entire success of achieving a solution depends on an efficient, vector-version, generalized unsymmetric eigensolver.

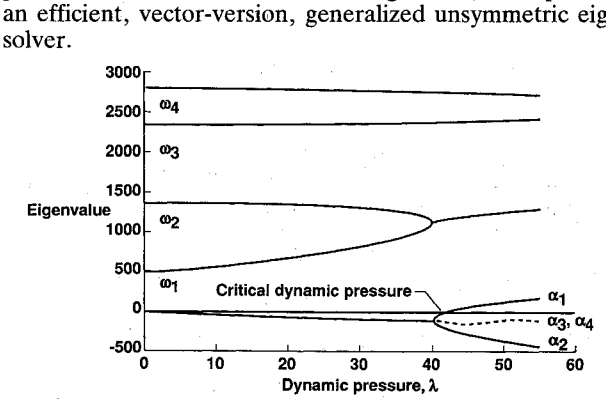


**Fig. 2 Linear panel flutter variation of eigenvalue for first four modes vs dynamic pressure for a square, simply-supported, B5.6/AL 6061-F panel ($\mu/M_\infty = 0.1$, $M_\infty h/a = 0.05$).**

## III. Development of Unsymmetric Eigensolver

### A. Orthogonal Reduction

Fortunately, only a few of the lowest eigenpairs are required for the solution during each iteration. This feature makes it possible to develop an efficient eigensolver for either large-amplitude vibration or the nonlinear flutter analysis. The eigenequation (10) can always be transformed into the standard form (a shift should be applied when necessary)

$$\mathbf{A}x = \mu x \tag{17}$$

where

$$\mathbf{A} = \begin{bmatrix} [G] & [K] \\ [-I] & [0] \end{bmatrix}^{-1} \begin{bmatrix} [-M] & [0] \\ [0] & [-I] \end{bmatrix} \tag{18a}$$

or

$$\mathbf{A} = \mathbf{B}^{-1}\mathbf{C} \tag{18b}$$

with

$$\mathbf{B} = \begin{bmatrix} [G] & [K] \\ [-I] & [0] \end{bmatrix}$$

$$\mathbf{C} = \begin{bmatrix} [-M] & [0] \\ [0] & [-I] \end{bmatrix} \tag{18c}$$

and the solution of Eq. (10) can be obtained as

$$\Omega = (1/\mu)$$

$$\{\Phi\} = \begin{Bmatrix} \Phi_1 \\ \Phi_2 \end{Bmatrix} = x \tag{19}$$

Since only a few of the lowest eigenpairs are required for Eq. (10) [or the largest for Eq. (17)], a reduction scheme that makes the largest ones converge first is preferred. This can be accomplished by defining the orthogonal transformation matrix $\mathbf{Q}_m (1 < m \leq n)$ as

$$A\mathbf{Q}_m = \mathbf{Q}_m + h_{m+1,m}q_{m+1}$$

$$\mathbf{Q}_m^T\mathbf{Q}_m = I_m \tag{20}$$

where $\mathbf{Q}_m = \{q_1, q_2, \ldots, q_m\}$, $\| q_i \| = 1$, $q_1$ is an arbitrary starting vector, and $q_{i+1}$ is determined through

$$h_{i+1,i}q_{i+1} = \mathbf{A}q_i - \sum_{k=1}^{i} h_{k,i}q_k, \qquad (h_{k,i} = q_i^T\mathbf{A}^Tq_k) \tag{21}$$

The reduced matrix $\mathbf{H}_m$ is an upper Hessenberg matrix

$$\mathbf{H}_m = \begin{bmatrix} h_{1,1} & h_{1,2} & h_{1,3} & \cdots & h_{1,m} \\ h_{2,1} & h_{2,2} & h_{2,3} & \cdots & h_{2,m} \\ 0 & h_{3,2} & h_{3,3} & \cdots & h_{3,m} \\ 0 & 0 & h_{4,3} & \cdots & h_{4,m} \\ \vdots & \vdots & \vdots & \vdots & \vdots \\ 0 & 0 & 0 & \cdots & h_{m,m} \end{bmatrix} \tag{22}$$

Due to the nature of the iteration[17] in Eq. (21), the reduced eigenequation

$$\mathbf{H}_m z = \Theta z \tag{23}$$

can be used to provide good approximate extreme eigenpairs of Eq. (10). The partial solution for Eq. (10) can be found from the transformation of the solution of Eq. (23), which can be obtained through the $QR$ method.[18] Thus, the solution procedure for Eq. (10) is summarized in Table 1. Given an arbitrary starting vector $\|\tilde{q}_0\| = 1$, then refine it for $\tilde{q}_{k+1} = \mathbf{A}\tilde{q}_k$ $(k = 0, 1, 2, 3)$ and let $q_1 = \tilde{q}_{k+1}/\|\tilde{q}_{k+1}\|$ before starting the actual iteration process.

**Table 1 Unsymmetric eigensolution procedure**

Step I: Reduction
For $J = 1$ to NMAX
$\tilde{q}_{J+1} = \mathbf{A}q_J$
For $k = 1$ to $J$
$\mathbf{H}(k, J) = \tilde{q}_{J+1}^T * q_k$
For $i = 1$ to $J$
$\tilde{q}_{J+1} = \tilde{q}_{J+1} - \mathbf{H}(i, J) * q_i$
$\mathbf{H}(J + 1, J) = \| \tilde{q}_{J+1} \|$
$q_{J+1} = (\tilde{q}_{J+1})/(\| \tilde{q}_{J+1} \|)$

Step II: Solve the reduced eigenequation
$\mathbf{H}_m\mathbf{z} = \Theta\mathbf{z}$

Step III: Calculate
$\mu = \Theta$
$\mathbf{x} = \mathbf{Q}\mathbf{z}$
$\Omega = 1/\Theta$
$\{\Phi\} = \mathbf{Q}\mathbf{z}$

**Table 2 Reduction with reorthogonalization**

I: Reduction
For $J = 1$ to NMAX
$\tilde{q}_{J+1} = \mathbf{A}q_J$
For $k = 1$ to $J$
$\mathbf{H}(k, J) = \tilde{q}_{J+1}^T * q_k$
For $i = 1$ to $J$
$\tilde{q}_{J+1} = \tilde{q}_{J+1} - \mathbf{H}(i, J) * q_i$
$\tilde{q}_{J+1} = (\tilde{q}_{J+1})/(\| \tilde{q}_{J+1} \|)$
Reorthogonalization of $q_{J+1}$
$\tilde{q}_{J+1} = q_{J+1} - (q_{J+1}^T * q_k) * q_k, \quad (k = 1, 2, \ldots, J)$
Determine $h_{j+1,j}$
$q_{J+1} = (\tilde{q}_{J+1})/(\| \tilde{q}_{J+1} \|)$
$\mathbf{H}(J + 1, J) = q_{J+1}^T\mathbf{A}q_J$

The proposed solver reduces the original eigenequation Eq. (17) to a significantly reduced solution space, Eq. (23), by employing the inverse power iteration and orthogonalization. The reduced eigenequation is solved by the $QR$ method, and the eigenvalues and eigenvectors of the original system are therefore obtained through appropriate transformations.

In practice, the $q$ vectors lose orthogonality very quickly; so that it is necessary to adopt reorthogonalization techniques in step 1 of Table 1. This technique is outlined in Table 2.

To illustrate the effect of using a refined starting vector and the re-orthogonalization technique on eigenvalues, nonlinear flutter analysis is performed on a simply supported 12 × 12 × 0.050 in. (30.5 × 30.5 × 0.127 cm) aluminum panel modeled with an 8 × 8 mesh (64 elements) where the original system of $n = 588$ is reduced to a system of $m = 40$. Table 3 shows this effect on eigenvalues with four options, and for convenience only the converged eigenpairs $[(\alpha_k, \omega_k), \Omega_k = \alpha_k + i\omega_k]$ are listed. The criteria for convergence requires the residual norm of Eq. (10) using the computed eigenvectors to be less than $10^{-7}$.

### B. Vectorization

Even though high-speed vector computers are available today, one cannot expect that real vector performance on such machines is granted. This means that the users are responsible for the vectorization of their codes, because the computer compiler can only vectorize limited simple do-loops.

To exploit the vector capability provided by modern high-performance computers, special attention should be given in

**Table 3 Effect of refined starting vector and reorthogonalization on eigenpairs ($\alpha_k$, $\omega_k$)**

| No. $k$ | Option 1[a] | Option 2[b] | Option 3[c] | Option 4[d] |
|---|---|---|---|---|
| 1 | (−1.785E-6, −742.99) | (0.0, −742.99) | — | — |
| 2 | (−1.785E-6, 742.99) | (0.0, 742.99) | — | — |
| 3 | (−1.661E-6, −1516.1) | — | — | — |
| 4 | (−1.661E-6, 1516.1) | — | — | — |
| 5 | (−1.567E-6, −1516.1) | — | (−1.567E-6, −1516.1) | — |
| 6 | (−1.567E-6, 1516.1) | — | (−1.567E-6, 1516.1) | — |
| 7 | (−1.517E-6, −2235.9) | — | — | — |
| 8 | (−1.517E-6, 2235.9) | — | — | — |
| 9 | (−1.375E-6, −2735.1) | — | — | — |
| 10 | (−1.375E-6, 2735.1) | — | — | — |
| 11 | (−1.472E-6, −3413.2) | — | — | — |
| 12 | (−1.472E-6, 3413.2) | — | — | — |
| 13 | (−1.868E-6, −4371.6) | — | — | — |
| 14 | (−1.868E-6, 4371.6) | — | — | — |
| 15 | (−4.891E-6, −4554.4) | — | — | — |
| 16 | (−4.891E-6, 4554.4) | — | — | — |

[a]Refine starting vector and reorthogonalization. [b]Refine starting vector and no reorthogonalization. [c]Arbitrary starting vector and reorthogonalization. [d]Arbitrary starting vector and no reorthogonalization.

designing a vectorable code. The common technique for doing this is so-called loop-unrolling,[19] which is introduced to minimize the CPU time required for loading and unloading data between registers and main memory. For example, the FORTRAN code for the matrix-vector operation ($y = Ax$) can be written as

```
      DO 100 J = 1, N
      DO 200 I = 1, N
      y(I) = y(I) + A(I, J)*x(J)
200 CONTINUE
100 CONTINUE
```

If the loop-unrolling technique is used, e.g., the loop-unrolling level is 2, then the above code should be changed to

```
      DO 100 J = 1, N, 2
      DO 200 I = 1, N
      y(I) = y(I) + A(I, J)*x(J)
                  + A(I, J+1)*x(J+1)
200 CONTINUE
100 CONTINUE
```

In this case, the loop-unrolling level equals to number of columns of matrix **A** being processed at the same time (in the same do-loop); thus, it is evident that higher loop-unrolling levels equals to a higher efficiency. In practice, however, the optimum loop-unrolling level is dependent on the vector-registers available on specific computer; for example, for the CRAY 2 and the CRAY Y-MP, it is 8 and for IBM 3090 it is 16.

For the orthogonal reduction procedure proposed here, not only matrix-vector operations, but also matrix factorization and forward/backward eliminations are involved. Thus, it is essential to arrange the data appropriately so that loop-unrolling is applicable. The storage scheme adopted here from matrix **B** in Eq. (18c) is so-called combined row- and column-oriented storage style.[20] For one-dimensional storage, the elements of B are stored as

$$\mathbf{B} = \{B(1, 1), B(1, 2), \ldots, B(1, n), B(2, 2),$$

$$B(2, 3), \ldots, B(2, n), B(3,3), \ldots, B(n, n), B(2, 1),$$

$$B(3, 1), \ldots, B(n, 1), B(3, 2), B(4, 2), \ldots,$$

$$B(n, 2), \ldots, B(n, n - 1)\}$$

Due to this special method of storage, loop-unrolling can be implemented for most operations; furthermore, the banded property of the matrix can be utilized to further reduce both CPU time and the storage space requirement. Table 4 shows the vector performance of matrix factorization on a CONVEX C220 computer. The CPU time for factorization is compared with the time given by the vectorized equation solver from the library subroutines installed on CONVEX C220.

**Table 4 Vector performance of factorization**

| Method | $n$ = NBWU[a] = NBWL[b] | CPU time, s |
|---|---|---|
| Present | 1452 | 67.25 |
| Solver in math/lib. | 1452 | 123.56 |

[a]NBWU = upper half-bandwidth of $B$. [b]NBWL = lower half-bandwidth of $B$.

**Table 5 Comparison of eigensolver methods and frequency ratio for several meshes for an inplane immovable clamped isotropic square plate[a]**

| Method | DOFs (mesh) | ($\omega_{nl}/\omega_l$) | CPU time, s / Iteration | No. of iterations |
|---|---|---|---|---|
| Present | 132 | 1.2150 | 0.842 | 6 |
| RGG | (4 × 4) | 1.2150 | 4.350 | 6 |
| Present | 644 | 1.1773 | 11.435 | 7 |
| RGG | (8 × 8) | 1.1773 | 476.214 | 7 |
| Present | 1540 | 1.1728 | 91.700 | 5 |
| RGG | (12 × 12) | 1.1728 | 8085.987 | 5 |
| Elliptic-integral method[22] | — | 1.1713 | — | — |
| Perturbation method[22] | — | 1.1731 | — | — |
| Incremental FEM[23] | — | 1.1762 | — | — |

[a]$E$ = 30 Msi (206.8 GPa), $\nu$ = 0.3, $\rho$ = 0.00026 lb-s$^2$/in.$^4$ (0.0028 kg/cm$^3$), $a$ = $b$ = 12 in. (30.5 cm), $h$ = 0.040 in. (0.1 cm) and $c/h$ = 1.0.

It should be noted that the vectorized solver was found to be about 10 times faster than a scalar solver for most modern computer systems. Combining both of these reduction and vectorization features, the proposed eigensolver was demonstrated to be a highly efficient tool for numerical analysis on modern, high-performance computers.

## IV. Results and Discussion

This unsymmetric eigenequation solver has been implemented and vectorized in a finite-element computer code for large-amplitude vibration and nonlinear panel flutter analyses. Numerical results were obtained using CONVEX C220 and compared with the results by using the RGG[21] eigensolver available in the mathematical library of the CONVEX C220 computer. The results were compared, and the required CPU times indicate a considerable reduction in execution time necessary to generate a reliable approximation of the eigenpairs by using the proposed unsymmetric eigensolver. It should be noted here, that to find the first few eigenpairs, the RGG eigensolver has to go through the complete eigensolutions.

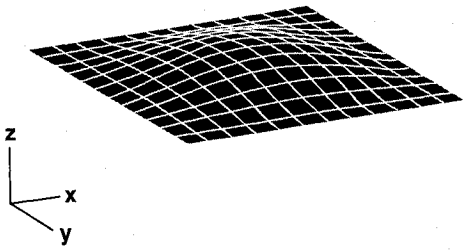


Fig. 3 Nonlinear first vibration mode shape for a square, clamped, isotropic panel.

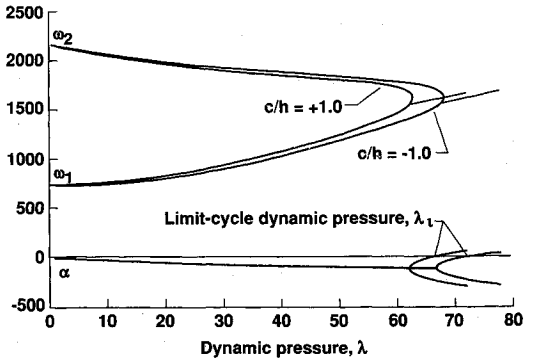


Fig. 4 Nonlinear panel flutter variation of eigenvalue for first two modes vs dynamic pressure for a square, simply supported, B5.6/AL 6061-F panel ($\mu/M_\infty = 0.1$, $M_\infty h/a = 0.05$).

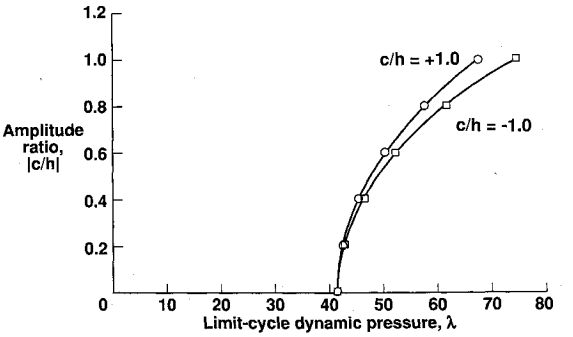


Fig. 5 Variation of limit-cycle amplitude vs limit-cycle dynamic pressure for a square, simply supported, B5.6/AL 6061-F panel ($\mu/M_\infty = 0.1$, $M_\infty h/a = 0.05$).

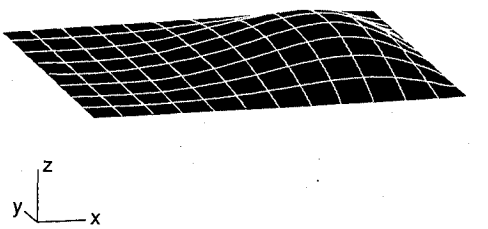


Fig. 6 Limit-cycle deflection shape of a square, simply supported, B5.6/AL 6061-F panel ($\mu/M_\infty = 0.1$, $M_\infty h/a = 0.05$, $\lambda = 67.71$, $c/h = +1.0$, 12 × 8 full panel).

Table 6 Finite-element mesh convergence and timing study for an in-plane immovable simply supported *B/Ep* three-dimensional square panel[a]

| Flutter model description | | | | | Present vector solver | | System solver on COVEX-220 RGG | |
|---|---|---|---|---|---|---|---|---|
| Mesh $n_i \times n_j$ | $N$ | NBWU | NBWL | $\lambda_l$ | CPU time, s per iteration | Total solution time, s | CPU time, s per iteration | Total solution time, s |
| 8 × 2 | 188 | 169 | 95 | 67.58 | 1.52 | 1,119.83 | 12.37 | 9,117.03 |
| 8 × 4 | 380 | 329 | 191 | 67.80 | 4.51 | 2,040.86 | 88.35 | 39,669.85 |
| 8 × 6 | 572 | 489 | 287 | 67.88 | 9.11 | 4,003.31 | 337.32 | * |
| 8 × 8 | 764 | 649 | 383 | 67.90 | 16.69 | 5,855.90 | 962.29 | * |
| 12 × 6 | 860 | 733 | 431 | 67.91 | 26.43 | 8,086.99 | 1,250.35 | * |
| 12 × 12 | 1,724 | 1,453 | 863 | 67.43 | 148.14 | 35,418.04 | 13,298.12 | * |

[a] $\mu/M_\infty = 0.1$, $M_\infty h/a = 0.05$ and $c/h = 1.0$. *Solution exceeded batch que time limit.

The large-amplitude vibration results ($\omega_{nl}/\omega_l$ is the nonlinear to linear frequency ratio) shown in Table 5, are for a square, clamped, inplane immovable, isotropic panel with a maximum deflection amplitude of one plate thickness.

Table 5 also shows the results of a convergence study to investigate the accuracy of the proposed finite-element method for a dynamic pressure of zero (in vacuo). These results indicate that a 8 × 8 full-plate mesh yields results that correlate extremely well with the elliptical integral and perturbation classical methods, as well as an incremental finite-element method. A plot of the nonlinear first mode shape for the 12 × 12 mesh is shown in Fig. 3.

Recall that about 150 eigensolutions are required during the nonlinear panel flutter analysis. Table 6 gives the CPU time for both eigensolution and the complete panel flutter analysis for different problem sizes.

Linear finite-element flutter results for a Boron Aluminum-B5.6/Al 6061-F[24] 8-layer $[0/90/0/90]_s$, square [$a$ = 12 in. (30.5 cm), $h$ = 0.040 in. (0.1 cm)], simply supported inplane immovable panel are shown in Fig. 2 for a damping parameter $\mu/M_\infty \simeq 0.1$ ($\mu = \rho_a a/ph$ = mass ratio). These results show the effect that increasing the dynamic pressure has on the first, second, third, and fourth system frequencies using first-order piston theory aerodynamics. The first and second modes coalesce at a dynamic pressure of approximately 40. However, since aerodynamic damping is present the critical dynamic pressure, $\lambda_{cr}$ is found to be 41.78 and no other modes were found to coalesce up to a dynamic pressure of 100.

The influence of the full third-order piston theory aerodynamics coupled with large-amplitude motion is shown in Fig. 4. The results presented in Fig. 4 are for a B5.6/Al 6061-F[24] 8-layer $[0/90/0/90]_s$, square [$a$ = 12 in. (30.5 cm), $h$ = 0.040 in. (0.1 cm)], simply supported inplane immovable panel. Also shown are the limit-cycle dynamic pressures for both ±1.0 amplitude ratio ($c/h$). Unlike the first-order piston theory, the third-order piston theory results for the same panel are dependent upon the sign of the amplitude, see Fig. 5. Similarly, the value of λ for which the real part of the eigenvalue vanishes can vary by as much as 8% for the cases evaluated in this study. A plot of the nonlinear flutter panel deflection for the $c/h = +1.0$ is shown in Fig. 6. Similar to the two-dimensional panel flutter results, the maximum amplitude was noted to occur at ¾ span for this case.

## V. Concluding Remarks

An analytical procedure for large-amplitude panel flutter at high supersonic/hypersonic speeds has been developed using the finite-element method. Extension of the finite-element three-dimensional panel flutter formulation to include both nonlinear third-order piston theory loading and composite

materials using classical laminated plate theory is presented. Results are presented that correlate the nonlinear finite-element method with classical large-amplitude vibration methods.

Results are also presented that show that the proposed unsymmetric eigensolver is efficient and takes full advantage of modern high-performance computer capabilities. This solver exploits the banded properties of the system matrices and utilizes an iterative reduction technique with refined starting vector and reorthogonalization to ensure convergence of the first few eigenpairs. Furthermore, compared with other reduction methods,[12] no complex matrix operations are involved in finding complex eigenpairs, and only right vectors need be calculated during the solution.

## Acknowledgments

This work is partially supported by NASA Langley Research Center under Grants NAS1-18584-38 and NAG1-858, and the Old Dominion University.

## References

[1]Laurenson, R. M., and McPherson, J. I., "Design Procedures for Flutter-Free Surface Panels," NASA CR-2801, March 1977.

[2]Cunningham, H. J., "Flutter of Flat Rectangular Panels Based on Three-Dimensional Supersonic Unsteady Potential Flow," NASA TR R-256, Feb. 1967.

[3]Dugundji, J., "Theoretical Considerations of Panel Flutter at High Supersonic Mach Numbers," *AIAA Journal*, Vol. 4, July 1966, pp. 1257–1266.

[4]Ashley, H., and Zartarian, G., "Piston Theory—A New Aerodynamic Tool for the Aeroelastician," *Journal of Aeronautical Sciences*, Vol. 23, Dec. 1956, pp. 1109–1118.

[5]McIntosh, S. G., Jr., "Theoretical Considerations of Some Nonlinear Aspects of Hypersonic Panel Flutter," Dept. of Aeronautics and Astronautics, Stanford Univ., Final Rept., Sept. 1, 1965 to Aug. 31, 1970, NASA Grant NGR 05-020-102, Stanford, CA, Nov. 1974.

[6]Dowell, E. H., "Panel Flutter: A Review of the Aeroelastic Stability of Plates and Shells," *AIAA Journal*, Vol. 8, March 1970, pp. 385–399.

[7]Reed, W. H., Hanson, P. W., and Alford, W. J., "Assessment of Flutter Model Testing Related to the National Aero-Space Plane," NASP CR 1002, NASA Langley Research Center, Hampton, VA, July 1987.

[8]Bathe, K. J., *Finite Element Procedures in Engineering*, Prentice-Hall, Englewood Cliffs, NJ, 1982.

[9]Lanczos, C., "An Iteration Method for the Eigenvalue Problem of Linear Differential and Integral Operators," *Journal Research of the National Bureau of Standards*, Vol. 45, No. 4, 1950, pp. 255–282.

[10]Qin, J., Nugyen, D. T., and Zhang, Y., "A Parallel-Vector Lanczos Eigensolver for Structural Vibration Problems," *Proceedings of the Fourth International Conference on Recent Advances in Structural Dynamics*, Southampton, England, UK, July 15–18, 1991, pp. 299–312.

[11]Yu, I.-W., "Solution of Large Unsymmetric Eigensystems for Fluid/Structure Interaction Problems," *Nuclear Science and Engineering*, Vol. 92, No. 1, 1986, pp. 157–161.

[12]Newman, M., and Mann, F. I., "Extension of the Tridiagonal Reduction (FEER) Method for Complex Eigenvalue Problems in NASTRAN," *7th NASTRAN User's Colloquium*, NASA CP-2062, Marshall Space Flight Center, Huntsville, AL, Oct. 1979, pp. 419–446.

[13]Kim, H. M., and Craig, R. R., Jr., "Computational Enhancement of an Unsymmetric Block Lanczos Algorithm," *International Journal for Numerical Methods in Engineering*, Vol. 30, No. 6, 1990, pp. 1083–1089.

[14]Wilkinson, J. H., *The Algebraic Eigenvalue Problem*, Oxford University Press, Oxford, England, UK, 1965.

[15]Jones, R. M., *Mechanics of Composite Materials*, McGraw-Hill, NY, 1975.

[16]Gray, C. E., Jr., Mei, C., and Shore, C. P., "A Finite Element Method for Large Amplitude Two-Dimensional Panel Flutter at Hypersonic Speeds," *AIAA Journal*, Vol. 29, Feb. 1991, pp. 290–298.

[17]Bodewig, E., *Matrix Calculus*, Interscience, NY, 1959.

[18]Francis, J. G. F., "The QR Transformation, Parts I and II," *Computer Journal*, Vol. 4, No. 3, 1961, pp. 265–271, and No. 4, 1962, 332–345.

[19]CRAY, *Mini Manual*, CR-1, NASA Langley Research Center, Hampton, VA, March 1989.

[20]Qin, J., Gray, C. E., Jr., Mei, C., and Nguyen, D. T., "A Parallel-Vector Equation Solver for Unsymmetric Matrices on Supercomputers," *Computing Systems in Engineering*, Vol. 2, Nos. 2 and 3, 1991, pp. 197–201.

[21]CONVEX, *Mathematical Libraries*, CX-3, CONVEX Computer Corp., Richardson, TX, July 1989.

[22]Gray, C. E., Jr., Decha-Umphai, K., and Mei, C., "Large Deflection, Large Amplitude Vibrations, and Random Response of Symmetrically Laminated Plates," *Journal of Aircraft*, Vol. 22, No. 11, 1985, pp. 929, 930.

[23]Lau, S. L., Cheung, Y. K., and Wu, S. Y., "Nonlinear Vibration of Thin Elastic Plates, Part I," *Journal of Applied Mechanics*, Vol. 51, Dec. 1984, pp. 837–844.

[24]*DOD/NASA Advanced Composite Design Guide*, 1st ed., AF Flight Dynamics Lab., Wright-Patterson AFB, OH, 1983.